micromachines

MDPI

Article

Design and Analysis of Gallium Nitride-Based p-i-n Diode Structure for Betavoltaic Cell with Enhanced Output Power Density

Young Jun Yoon [1], Jae Sang Lee [1], In Man Kang [2], Jung Hee Lee [2] and Dong Seok Kim [1,*]

[1] Korea Multi-Purpose Accelerator Complex, Korea Atomic Energy Research Institute, Gyeongju 38180, Korea; yjyoon@kaeri.re.kr (Y.J.Y.); jslee8@kaeri.re.kr (J.S.L.)

[2] School of Electronic and Electrical Engineering, Kyungpook National University, Daegu 41566, Korea; imkang@ee.knu.ac.kr (I.M.K.); jlee@ee.knu.ac.kr (J.H.L.)

* Correspondence: dongseokkim@kaeri.re.kr; Tel.: +82-054-750-5310

Received: 20 November 2020; Accepted: 11 December 2020; Published: 12 December 2020

Abstract: In this work, Gallium Nitride (GaN)-based p-i-n diodes were designed using a computer aided design (TCAD) simulator for realizing a betavoltaic (BV) cell with a high output power density (P_{out}). The short-circuit current density (J_{SC}) and open-circuit voltage (V_{OC}) of the 17 keV electron-beam (e-beam)-irradiated diode were evaluated with the variations of design parameters, such as the height and doping concentration of the intrinsic GaN region ($H_{i\text{-}GaN}$ and $D_{i\text{-}GaN}$), which influenced the depletion width in the i-GaN region. A high $H_{i\text{-}GaN}$ and a low $D_{i\text{-}GaN}$ improved the P_{out} because of the enhancement of absorption and conversion efficiency. The device with the $H_{i\text{-}GaN}$ of 700 nm and $D_{i\text{-}GaN}$ of 1×10^{16} cm^{-3} exhibited the highest P_{out}. In addition, the effects of native defects in the GaN material on the performances were investigated. While the reverse current characteristics were mainly unaffected by donor-like trap states like N vacancies, the Ga vacancies-induced acceptor-like traps significantly decreased the J_{SC} and V_{OC} due to an increase in recombination rate. As a result, the device with a high acceptor-like trap density dramatically degenerated the P_{out}. Therefore, growth of the high quality i-GaN with low acceptor-like traps is important for an enhanced P_{out} in BV cell.

Keywords: betavoltaic cell; Gallium Nitride (GaN); high-output power; TCAD simulation

1. Introduction

Betavoltaic (BV) cells using a radioisotope have been developed for micro-battery applications, such as a power source of bio-medical implants and extreme environmental sensors [1–3], because of their long lifetime and micro-size. ^{63}Ni radioisotope–based BV cells can be used for a long period due to a half-life of about 100 years. The BV cells based on various semiconductors such as Si [4,5], GaAs [6], SiC [7–9], GaN [10–14], and GaP [15] have been studied for high power conversion efficiency. Among the semiconductors, it is known that GaN-based BV cells can theoretically obtain superior conversion efficiency because of a wider energy bandgap. Moreover, GaN-based BV cells are more suitable for BV applications with long-term stability because GaN material has exhibited a strong radiation hardness [16,17], which can reduce the effects of radiation damage on device performances [18]. The p-i-n junction [10–12] and Schottky barrier diode [13,14] have been used to realize GaN-based BV cells. The p-i-n junction diode can obtain a wider depletion width, which improves the collection efficiency. However, the efficiency of the fabricated device exhibited a lower power conversion efficiency than the theoretical efficiency. Recent studies on BV cells aimed at enhancing the conversion efficiency. Many researchers have made progress in the optimization design of diode structures using

a theoretical calculation model [19,20]. However, the design considerations of the GaN-based BV cells still have to be addressed due to the inherent properties of GaN material, including the various native trap states that occur during growth. The short-circuit current density (J_{SC}) and open-circuit voltage (V_{OC}) associated with the output power density of the diode are significantly affected by the native defects that influence recombination.

In this work, we optimized the GaN-based p-i-n diode to achieve a BV cell with high output power density using the following design parameters: heights of p-type GaN and intrinsic GaN ($H_{p\text{-}GaN}$ and $H_{i\text{-}GaN}$) and a doping concentration of i-GaN ($D_{i\text{-}GaN}$). The physical phenomenon and performance were analyzed using a three-dimensional (3-D) technology computer-aided design (TCAD) simulator with physical models including e-beam irradiation and trap-assisted recombination models. The effects of native defects on J_{SC}, V_{OC}, and P_{out} of the e-beam-irradiated devices were also investigated.

2. Device Structure and Simulation Method

Figure 1 shows the 3-D schematic of the GaN-based p-i-n diode for BV cells. The p-i-n diode structure is the conventional diode structure, which consisted of an intrinsic GaN (i-GaN) region between p-type GaN (p-GaN) and n-type GaN (n-GaN) regions to obtain a wide width in the depletion region. The $D_{i\text{-}GaN}$ determines the depletion width, which affects the conversion efficiency for BV cells. Here, i-GaN denotes undoped GaN, which is almost an n-type due to the residual donor [21]. The background impurity concentration in undoped GaN grown by metal-organic chemical-vapor deposition (MOCVD) is typically in the range of 10^{15} to 10^{17} cm^{-3}, depending on the condition of the reactor [22]. Furthermore, it is difficult to grow undoped GaN with simultaneous low doping concentration and high quality [23]. Thus, the $D_{i\text{-}GaN}$ was varied in the range of 5×10^{15} cm^{-3} to 5×10^{16} cm^{-3} for optimizing the $D_{i\text{-}GaN}$. In order to reduce the resistance of the n-GaN and p-GaN layers, doping concentrations of the n-GaN and p-GaN ($D_{n\text{-}GaN}$ and $D_{p\text{-}GaN}$) were designed as 5×10^{18} cm^{-3} and 5×10^{17} cm^{-3}, respectively. We also changed the $H_{p\text{-}GaN}$ and $H_{i\text{-}GaN}$ to achieve high performance. The variation ranges of $H_{p\text{-}GaN}$ and $H_{i\text{-}GaN}$ were 60–200 nm and 500–900 nm, respectively. The ranges of $H_{p\text{-}GaN}$ and $H_{i\text{-}GaN}$ values were determined by considering the penetration depth of 17 keV electrons at about 1 μm [24]. The energy of the e-beam is the average energy of ^{63}Ni [25,26]. The contact resistance for p-GaN and n-GaN in the devices was 1×10^{-4} Ω·cm^2 [27,28].

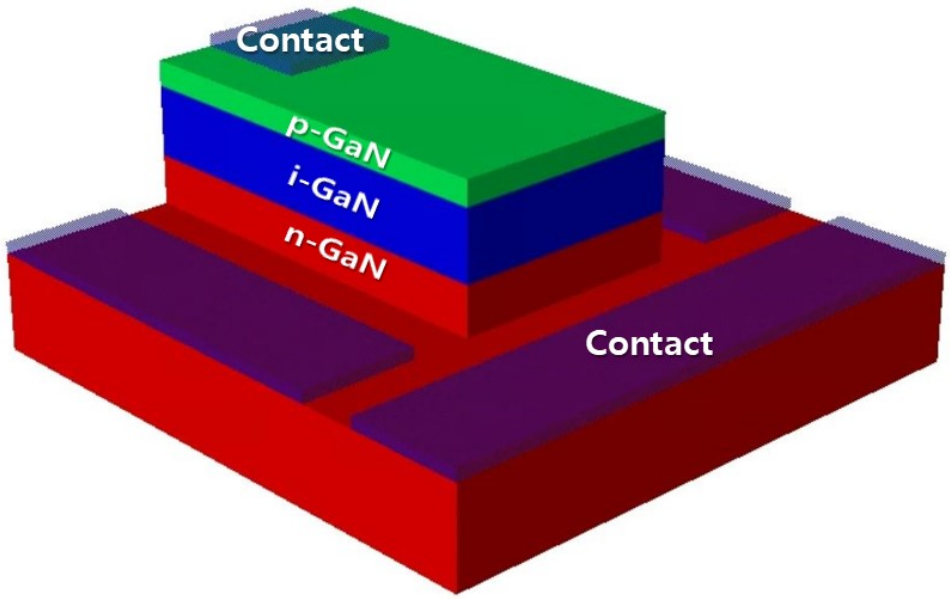

Figure 1. 3-D schematic of the p-i-n diode structure for betavoltaic (BV) cell.

The effects of e-beam irradiation on current characteristics were analyzed using a TCAD simulator [29]. Physical models were applied in the simulation, including Schockley–Read–Hall (SRH) and trap-assisted tunneling (TAT), and a low-field mobility model. The SRH and TAT models were used to reflect the carrier recombination phenomenon [30], which significantly affects the J_{SC} and V_{OC} of the diode. For the effects of native defects in the GaN material [31,32], acceptor and donor-like trap states were added to the simulation. The acceptor-like trap state is formed by Ga vacancies. The donor-like trap states are mainly associated with the N vacancies and nitrogen antisite point defect. When we optimized the structure, we analyzed the performances of the diodes applied by native traps. In addition, the individual impact of trap states on P_{out} were studied to investigate the dominant traps that degrade the performances.

3. Results and Discussion

Figure 2a shows the effects of e-beam irradiation on the reverse current characteristics of the GaN p-i-n diode. When the diode was irradiated by a 17 keV e-beam, the reverse current density significantly increased. This was because electron-hole pairs (EHPs) were generated by the injected high-energy electrons. The electrons and holes in the depletion region were respectively moved by internal electric field through n-GaN and p-GaN regions and the carriers converted to the electric current. The J_{SC} and a V_{OC} of the irradiated diode were 14.92 μA/cm^2 and 2.391 V, respectively. The J_{SC} and V_{OC} were defined as the current density at a voltage of 0 V and the voltage when the current density was 0 A/cm^2, respectively.

As shown in Figure 2b, the 17 keV electrons penetrated up to a depth of about 1 μm and the peak absorption rate was exhibited at a depth of about 300 nm. Because many EHPs generated in the i-GaN region contributed to the conversion efficiency, the $H_{i\text{-}GaN}$ and $D_{i\text{-}GaN}$ are important design parameters. A high conversion efficiency increases J_{SC} and V_{OC}, which influences the output power density (P_{out}). The diode exhibited the maximum P_{out} (P_{out_max}) at a voltage of 2.18 V, as shown in Figure 2c.

Figure 3a shows the variations of the reverse current characteristics of the irradiation diodes as a function of $H_{i\text{-}GaN}$. As the $H_{i\text{-}GaN}$ increased, the reverse current density became higher due to extension of the absorption region. Many EHPs were generated in the extended absorption region, which converted the electric current. However, the current density of the diodes with a $H_{i\text{-}GaN}$ above 900 nm was lower than that of the device with a $H_{i\text{-}GaN}$ of 700 nm at a forward voltage above 0 V. This result indicated that excess carriers generated by the e-beam were reduced by the recombination mechanism as they moved through the n-GaN or p-GaN regions. This result affected the V_{OC} and J_{SC} of the diodes. As shown in Figure 3b, the device with a $H_{i\text{-}GaN}$ of 700 nm had the highest V_{OC}. In terms of P_{out_max}, the device with a $H_{i\text{-}GaN}$ of 700 nm exhibited the highest P_{out_max} because the device was less affected by the recombination phenomenon, as shown in Figure 3c.

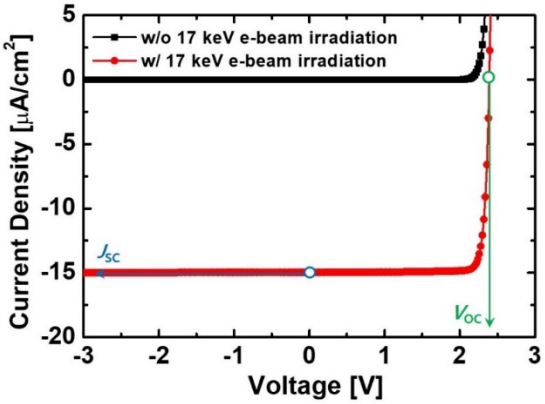

(**a**)

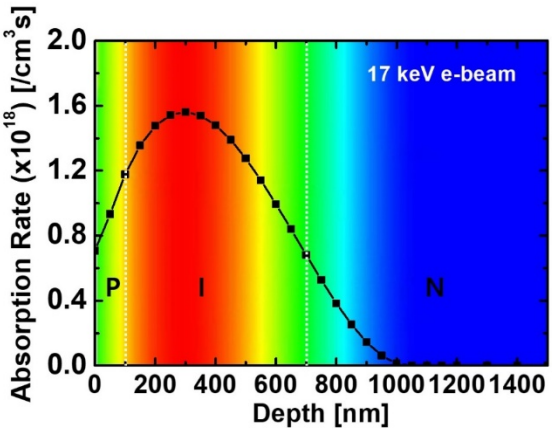

(**b**)

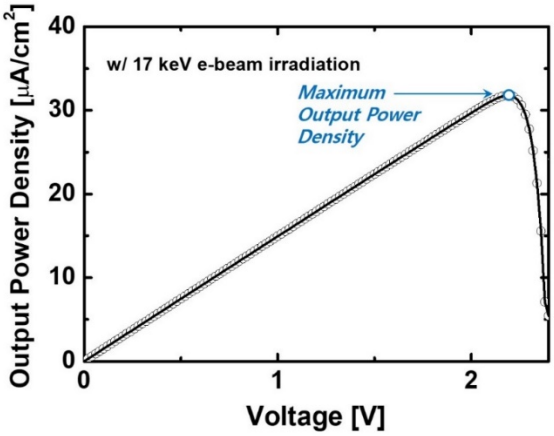

(**c**)

Figure 2. (**a**) Effects of e-beam irradiation on reverse current characteristics of the diode. (**b**) Absorption rate vs. penetration depth in the diode for 17 keV e-beam irradiation. (**c**) The output power density of the e-beam-irradiated diode. $H_{\text{p-GaN}}$ and $H_{\text{i-GaN}}$ in the diode were 100 nm and 600 nm, respectively. $D_{\text{p-GaN}}$, $D_{\text{i-GaN}}$, and $D_{\text{n-GaN}}$ were 5×10^{17} cm^{-3}, 1×10^{16} cm^{-3}, and 5×10^{18} cm^{-3}, respectively.

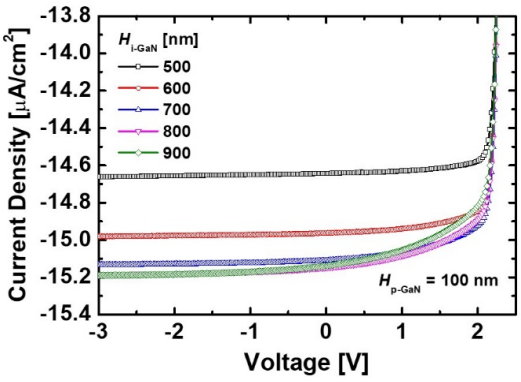

(**a**)

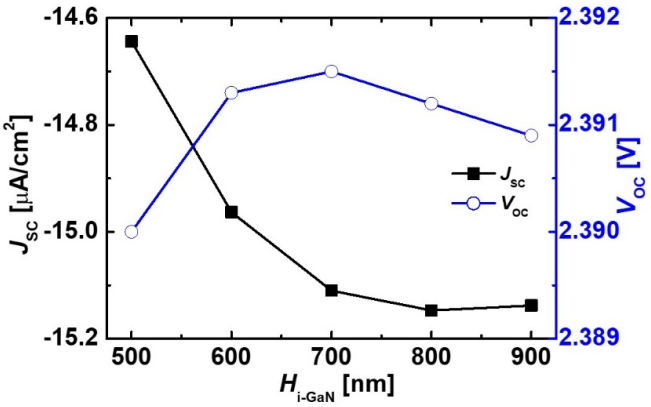

(**b**)

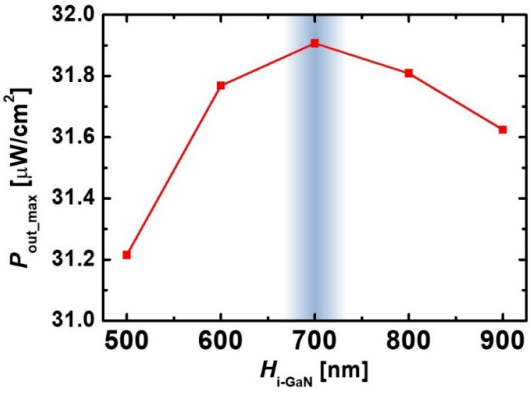

(**c**)

Figure 3. (**a**) Reverse current characteristics of the irradiated diodes with different $H_{\text{i-GaN}}$ values. (**b**) Variations of J_{SC}, V_{OC} and (**c**) $P_{\text{out\_max}}$ as a function of $H_{\text{i-GaN}}$. The $H_{\text{p-GaN}}$ was fixed as 100 nm. The $D_{\text{p-GaN}}$, $D_{\text{i-GaN}}$, and $D_{\text{n-GaN}}$ were 5×10^{17} cm^{-3}, 1×10^{16} cm^{-3}, and 5×10^{18} cm^{-3}, respectively.

The variations of J_{SC}, V_{OC}, and $P_{\text{out\_max}}$ depending on the $H_{\text{i-GaN}}$ and $H_{\text{p-GaN}}$ are shown in Figure 4. The J_{SC} of the devices increased with a rise in the $H_{\text{i-GaN}}$ regardless of the $H_{\text{p-GaN}}$ because a high $H_{\text{i-GaN}}$ extended the absorption region. When the $H_{\text{i-GaN}}$ above 800 nm increased, the J_{SC} slightly decreased due to the recombination phenomenon. As the $H_{\text{p-GaN}}$ became shorter, the variation of J_{SC} according to the $H_{\text{i-GaN}}$ increased. This result indicated that the absorption rate vs. depth was more affected in the irradiated device with a short $H_{\text{p-GaN}}$. The device with a $H_{\text{p-GaN}}$ of 60 nm and $H_{\text{i-GaN}}$ of 800 nm was the highest J_{SC} because the J_{SC} was enhanced by an additional absorption near the p-GaN

region. In case of the V_{OC}, the device with a $H_{p\text{-}GaN}$ of 100 nm and a $H_{i\text{-}GaN}$ of 700 nm exhibited the highest V_{OC}, as shown in Figure 4b. Because a short $H_{p\text{-}GaN}$ degenerated the carrier transport, the V_{OC} of the devices with a $H_{p\text{-}GaN}$ of 60 nm was a smaller than that of the devices with a $H_{p\text{-}GaN}$ of 100 nm. The device also obtained the highest P_{out_max}. The P_{out_max} value was affected by a change of the V_{OC}.

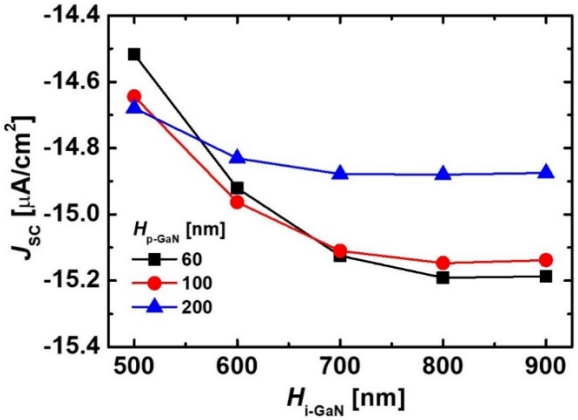

(**a**)

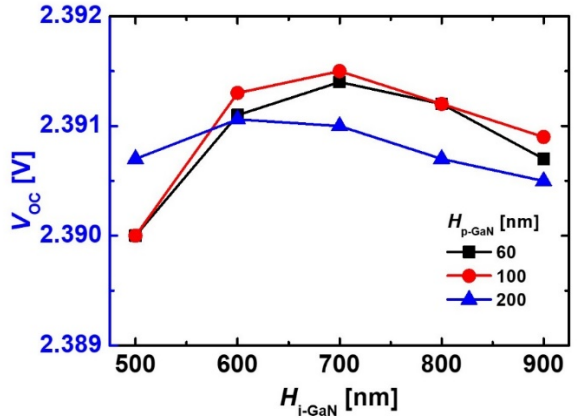

(**b**)

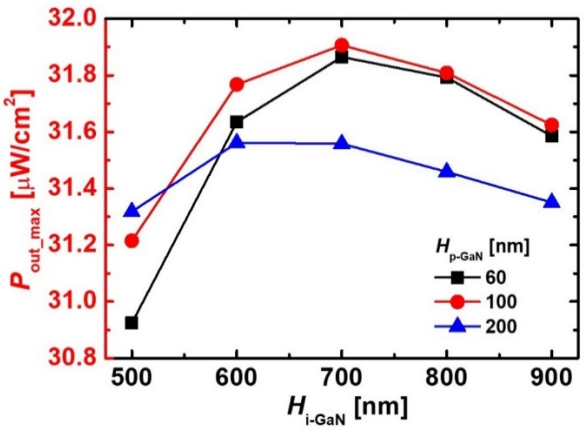

(**c**)

Figure 4. Variations of (**a**) J_{SC}, (**b**) V_{OC} and (**c**) P_{out_max} of the irradiated diodes dependent on the $H_{i\text{-}GaN}$ and $H_{p\text{-}GaN}$. The $D_{p\text{-}GaN}$, $D_{i\text{-}GaN}$, and $D_{n\text{-}GaN}$ were 5×10^{17} cm^{-3}, 1×10^{16} cm^{-3}, and 5×10^{18} cm^{-3}, respectively.

Figure 5 shows energy band diagrams of the diodes with different values of $D_{i\text{-}GaN}$. As the $D_{i\text{-}GaN}$ decreased, the depletion region was extended in the i-GaN region. Because the depletion region was influenced by the $D_{i\text{-}GaN}$, we examined the variations of J_{SC}, V_{OC} and P_{out_max} depending on the $D_{i\text{-}GaN}$ and $H_{i\text{-}GaN}$. As shown in Figure 6, the diode with a low $D_{i\text{-}GaN}$ exhibited an improved J_{SC} because of a wider depletion region in the i-GaN region. The excess carriers could be moved by the built-in electric field. Although the device with a $D_{i\text{-}GaN}$ of 1×10^{16} cm^{-3} exhibited a higher V_{OC}, the diode with a $D_{i\text{-}GaN}$ of 5×10^{15} cm^{-3} obtained a higher P_{out_max}. This result indicated that reducing the $D_{i\text{-}GaN}$ is important to improving transport efficiency. However, in terms of GaN epitaxial technology based on MOCVD method, it was difficult to reduce the $D_{i\text{-}GaN}$ below 1×10^{16} cm^{-3} because residual impurities remained during the growth process. Therefore, we determined that the optimum point for the $D_{i\text{-}GaN}$ was 1×10^{16} cm^{-3}. As a result, the diode structure with a $H_{p\text{-}GaN}$ of 100 nm, $H_{i\text{-}GaN}$ of 700 nm, and $D_{i\text{-}GaN}$ of 1×10^{16} cm^{-3} was optimized, and the effects of native trap states on performances of the optimized diode were investigated with variations of trap level and density.

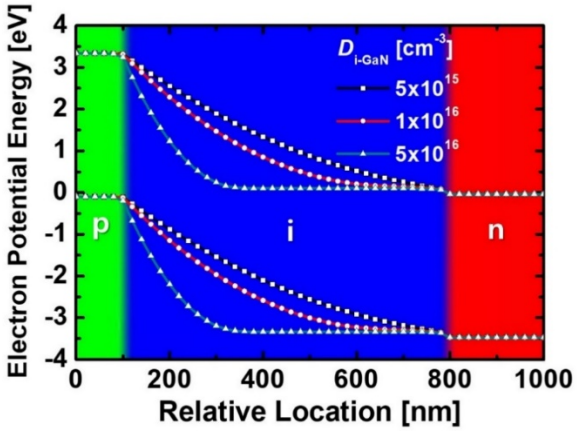

Figure 5. Energy band diagrams of the diodes with different values of $D_{i\text{-}GaN}$. All the devices were designed with a $H_{p\text{-}GaN}$ of 100 nm and a $H_{i\text{-}GaN}$ of 700 nm. The $D_{p\text{-}GaN}$ and $D_{n\text{-}GaN}$ of the devices were 5×10^{17} cm^{-3} and 5×10^{18} cm^{-3}, respectively.

The energy spectrum of the ^{63}Ni source exhibited a wide range to a 66 keV peak energy [19]. We additionally confirmed the performances of the optimized diode depending on the injected electron energy. The current characteristics of the diodes irradiated by different e-beam energies is shown in Figure 7a. As the energy increased up to 30 keV, the current became higher. This was because many EHPs were generated by a wide distribution of absorption rate as shown in Figure 7b. However, when the electrons with an energy above 40 keV were injected, the current of the irradiated device was lower than that of the device irradiated by the 17 keV e-beam. These results revealed that the variations of the current of the irradiated diodes depending on the energy of the e-beam were large. The probability of beta particles generated from the ^{63}Ni source showed a high distribution below 20 keV [19]. Also, the depletion width formed in the i-GaN region was small at about 600 nm (in case of $D_{i\text{-}GaN} = 1 \times 10^{16}$ cm^{-3}), and the diffusion length of GaN can be shortened by native defects. Therefore, in order to achieve a high efficiency BV cell using the ^{63}Ni source, it is necessary to analyze the performances of GaN-based diodes considering the spectrum of the ^{63}Ni source.

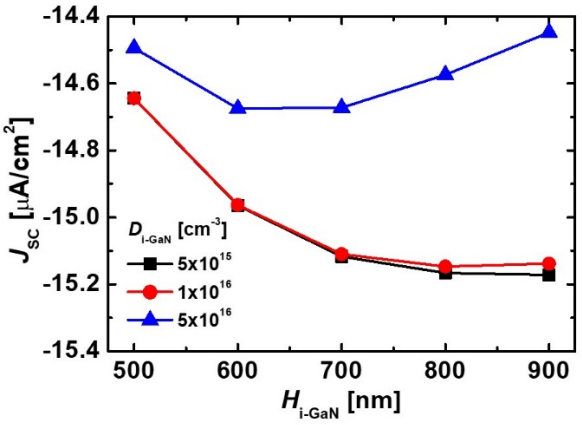

(**a**)

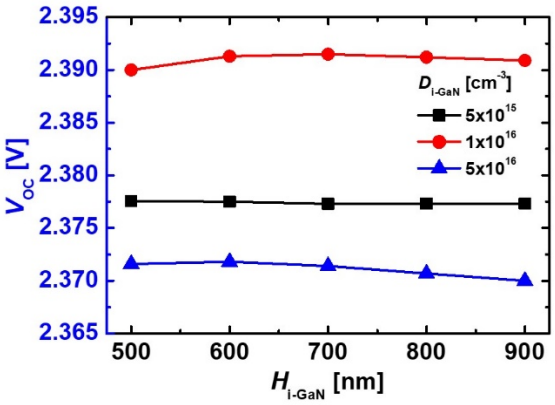

(**b**)

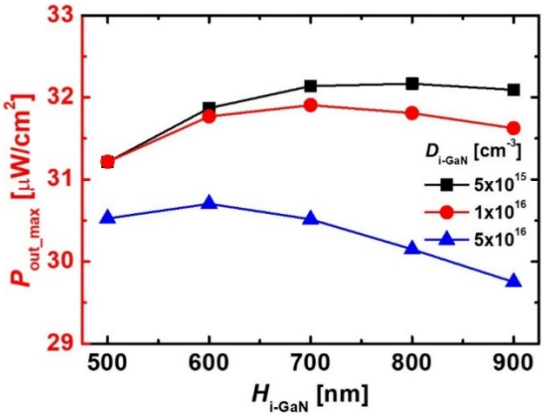

(**c**)

Figure 6. Variations of (**a**) J_{SC}, (**b**) V_{OC} and (**c**) P_{out_max} of the e-beam-irradiated diodes depending on $H_{i\text{-}GaN}$ and $D_{i\text{-}GaN}$. All devices were designed with a $H_{p\text{-}GaN}$ of 100 nm and $H_{i\text{-}GaN}$ of 700 nm. The $D_{p\text{-}GaN}$ and $D_{n\text{-}GaN}$ of the devices were 5×10^{17} cm^{-3} and 5×10^{18} cm^{-3}, respectively.

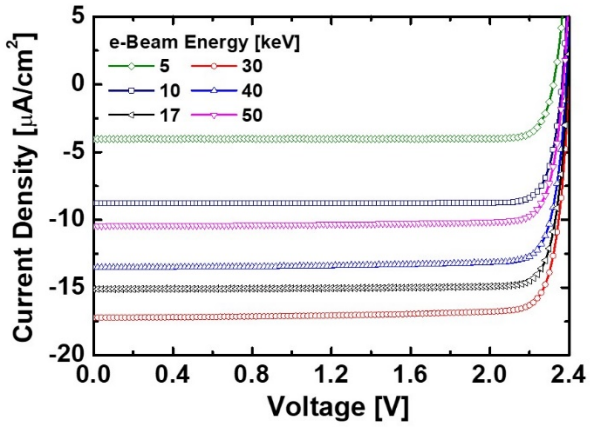

(**a**)

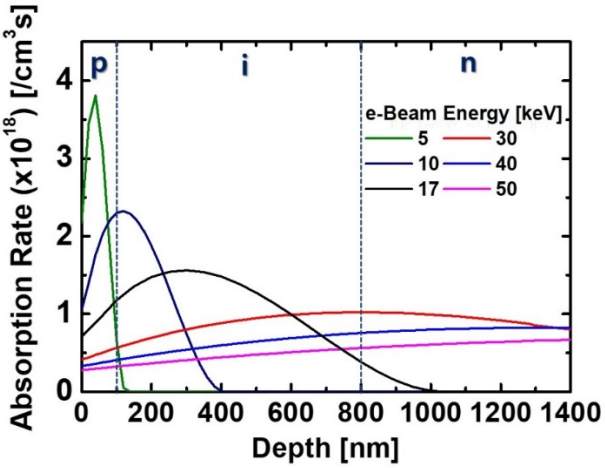

(**b**)

Figure 7. (**a**) Current characteristics of the diodes irradiated by different e-beam energies and (**b**) absorption rate varied by different e-beam energies. All devices were designed with a $H_{\text{p-GaN}}$ of 100 nm and $H_{\text{i-GaN}}$ of 700 nm. The $D_{\text{p-GaN}}$ and $D_{\text{n-GaN}}$ of the devices were 5×10^{17} cm^{-3} and 5×10^{18} cm^{-3}, respectively.

Figure 8 shows reverse current density and P_{out} of the irradiated diodes with and without the native trap states including donor and acceptor-like traps. The reverse current density was significantly degenerated by the trap states. This result means that the trap-assisted recombination was caused by the native defects in the GaN material. As a result, the P_{out} of the device with the trap states was lower than that of the device without the trap states. We confirmed the effects of individual traps on current characteristics of the irradiated devices. As a shown in Figure 9, the impact of acceptor-like trap states was stronger than that of donor-like trap states. This result proved that the acceptor-like trap states represented the dominant factor for the recombination.

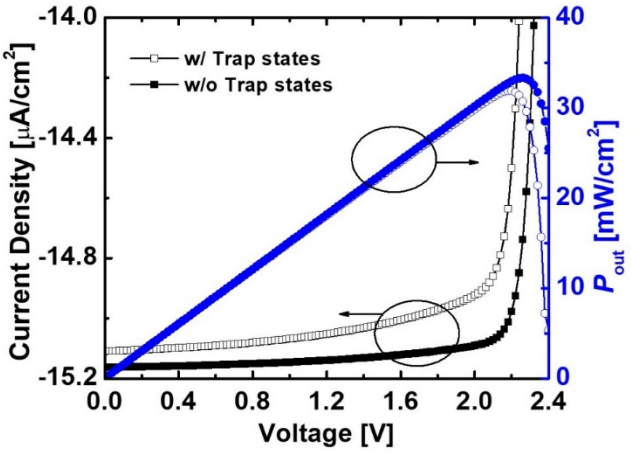

Figure 8. Current characteristics and P_{out} of the e-beam-irradiated diodes without and with native trap states. The $H_{p\text{-}GaN}$ and $H_{i\text{-}GaN}$ in the diode were 100 nm and 700 nm, respectively. $D_{p\text{-}GaN}$, $D_{i\text{-}GaN}$, and $D_{n\text{-}GaN}$ were 5×10^{17} cm^{-3}, 1×10^{16} cm^{-3}, and 5×10^{18} cm^{-3}, respectively.

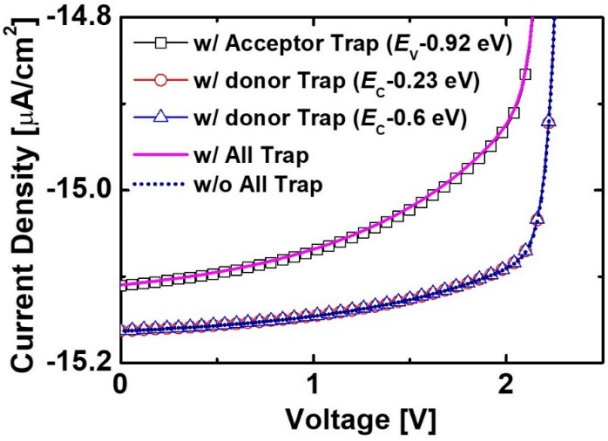

Figure 9. Effects of trap states on current characteristics of the e-beam-irradiated diodes. The $H_{p\text{-}GaN}$ and $H_{i\text{-}GaN}$ in the diode were 100 nm and 700 nm, respectively. $D_{p\text{-}GaN}$, $D_{i\text{-}GaN}$, and $D_{n\text{-}GaN}$ were 5×10^{17} cm^{-3}, 1×10^{16} cm^{-3}, and 5×10^{18} cm^{-3}, respectively.

In addition, we investigated the effects of trap density on J_{SC}, V_{OC}, and P_{out_max}. As the trap density increased, the performances were totally degenerated by the acceptor-like trap state, as shown in Figure 10. The donor-like trap states reduced the J_{SC} less than the acceptor-like trap state. While the donor-like trap states (E_C-0.6 eV) slightly decreased the V_{OC}, the shallow donor-like trap states (E_C-0.23 eV) increased V_{OC}. As a result, the P_{out_max} was unaffected by the shallow donor-like trap states (E_C-0.23 eV). It is important to reduce the acceptor-like traps to improve the conversion efficiency of the betavoltaic cell.

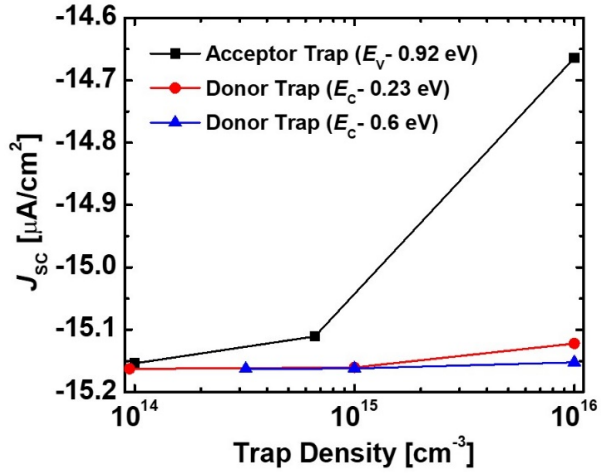

(**a**)

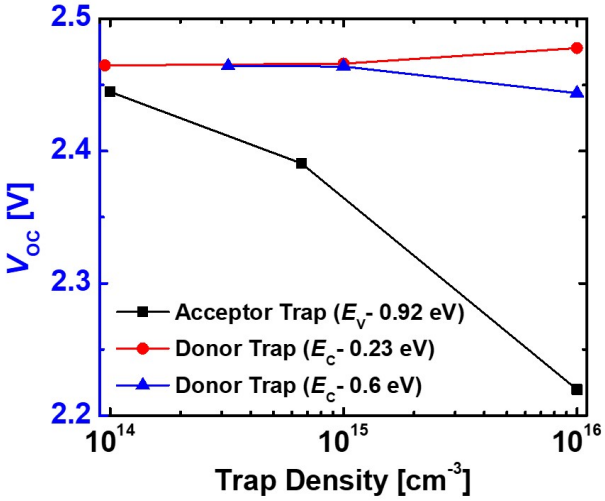

(**b**)

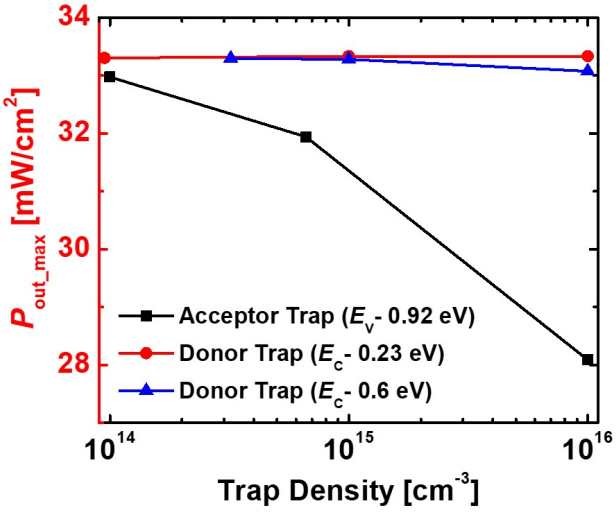

(**c**)

Figure 10. Effects of each donor and acceptor trap states on (**a**) J_{SC}, (**b**) V_{OC}, and (**c**) P_{out_max} of the e-beam-irradiated diodes. The $H_{p\text{-}GaN}$ and $H_{i\text{-}GaN}$ in the diode were 100 nm and 700 nm, respectively. $D_{p\text{-}GaN}$, $D_{i\text{-}GaN}$, and $D_{n\text{-}GaN}$ were 5×10^{17} cm^{-3}, 1×10^{16} cm^{-3}, and 5×10^{18} cm^{-3}, respectively.

4. Conclusions

In this work, we designed a p-i-n diode with a variation of geometric parameters, namely, $H_{\text{i-GaN}}$, $D_{\text{i-GaN}}$, and $H_{\text{p-GaN}}$, and analyzed P_{out} using 17 keV e-beam irradiation. The $H_{\text{i-GaN}}$ and $H_{\text{p-GaN}}$ affected the absorption rate vs. depth. A low $D_{\text{i-GaN}}$ produced an increase in depletion width. The optimized structure with a $H_{\text{i-GaN}}$ of 700 nm, $D_{\text{i-GaN}}$ of 1×10^{16} cm^{-3}, and $H_{\text{p-GaN}}$ of 100 nm obtained an improved P_{out}. In addition, the effects of native trap states on reverse current characteristics were investigated with various trap levels and densities. When the acceptor-like trap density increased from 10^{14} cm^{-3} to 10^{16} cm^{-3}, the trap significantly decreased the $P_{\text{out\_max}}$ by about 15%. GaN with low acceptor-like traps was needed to enhance the P_{out} of a BV cell. These results provide design considerations for achieving a high efficiency BV cell.

Author Contributions: Conceptualization, Y.J.Y. and D.S.K.; Investigation, Y.J.Y.; Data analysis, Y.J.Y., J.S.L., I.M.K., J.H.L., and D.S.K.; writing—original draft preparation, Y.J.Y.; writing—review and editing, D.S.K. All authors have read and agreed to the published version of the manuscript.

Funding: This work was supported by the National Research Foundation of Korea (NRF) grant (No. NRF-2018M2A2B3A01072437) funded by the Korea government-MSIT (Ministry of Science and ICT).

Conflicts of Interest: The authors declare no conflict of interest.

References

1. Prelas, M.A.; Weaver, C.L.; Watermann, M.L.; Lukosi, E.D.; Schott, R.J.; Wisniewski, D.A. A review of nuclear batteries. *Prog. Nucl. Energy* **2014**, *75*, 117–148. [CrossRef]
2. Spickler, J.W.; Rasor, N.S.; Kezdi, P.; Misra, S.N.; Robins, K.E.; Leboeuf, C. Totally self-contained intracardiac pacemaker. *J. Electrocardiol.* **1970**, *3*, 325–331. [CrossRef]
3. Ko, W.H.; Hynecek, J. Implant evaluation of a nuclear power source-betacel battery. *IEEE Trans. Biomed. Eng.* **1974**, *3*, 238–241. [CrossRef] [PubMed]
4. Rappaport, P. The Electron-Voltaic Effect in p-n Junctions Induced by Beta-Particle Bombardment. *Phys. Rev.* **1954**, *93*, 246–247. [CrossRef]
5. Uhm, Y.R.; Choi, B.G.; Kim, J.B.; Jeong, D.-H.; Son, K.J. Study of a Betavoltaic Battery Using Electroplated Nickel-63 on Nickel Foil as a Power Source. *Nucl. Eng. Technol.* **2016**, *48*, 773–777. [CrossRef]
6. Butera, S.; Lioliou, G.; Barnett, A.M. Temperature effects on gallium arsenide 63Ni betavoltaic cell. *Appl. Radiat. Isot.* **2017**, *125*, 42–47. [CrossRef]
7. Chandrashekhar, M.V.S.; Thomas, C.I.; Li, H.; Spencer, M.G.; Lal, A. Demonstration of a 4H SiC betavoltaic cell. *Appl. Phys. Lett.* **2006**, *88*, 033506. [CrossRef]
8. Thomas, C.; Portnoff, S.; Spencer, M.G. High efficiency 4H-SiC betavoltaic power sources using tritium radioisotopes. *Appl. Phys. Lett.* **2016**, *108*, 013505. [CrossRef]
9. Simulation and Optimization Design of SiC-Based PN Betavoltaic Microbattery Using Tritium Source. *Crystals* **2020**, *10*, 105. [CrossRef]
10. Munson, C.E.; Arif, M.; Streque, J.; Belahsene, S.; Martinez, A.; Ramdane, A.; Gmili, Y.E.; Salvestrini, J.-P.; Voss, P.L.; Ougazzaden, A. Model of Ni-63 battery with realistic PIN structure. *J. Appl. Phys.* **2015**, *118*, 105101. [CrossRef]
11. Khan, M.R.; Smith, J.R.; Tompkins, R.P.; Kelley, S.; Litz, M.; Russo, J.; Leathersich, J.; Shahedipour-Sandvik, R.; Jones, K.A.; Iliadis, A. Design and characterization of GaN p-i-n diodes for betavoltaic devices. *Solid-State Electron.* **2017**, *136*, 24–29. [CrossRef]
12. Munson, C.E.; Gaimard, Q.; Merghem, K.; Sundaram, S.; Rogers, D.J.; Sanoit, J.; Voss, P.L.; Ramdane, A.; Salvestrini, J.P.; Ougazzaden, A. Modeling, design, fabrication and experimentation of a GaN-based, 63Ni betavoltaic battery. *J. Phys. D Appl. Phys.* **2018**, *51*, 035101. [CrossRef]
13. Lu, M.; Zhang, G.-G.; Fu, K.; Yu, G.-H.; Su, D.; Hu, J.-F. Gallium Nitride Schottky betavoltaic nuclear batteries. *Energy Convers. Manag.* **2011**, *52*, 1955–1958. [CrossRef]
14. San, H.; Yao, S.; Wang, X.; Cheng, Z.; Chen, X. Design and simulation of GaN based Schottky betavoltaic nuclear micro-battery. *Appl. Radiat. Isot.* **2013**, *80*, 17–22. [CrossRef] [PubMed]
15. McNamee, S.; Wagner, D.; Fiordaliso, E.M.; Novog, D.; LaPierre, R.R. GaP nanowire betavoltaic device. *Nanotechnology* **2019**, *30*, 075401. [CrossRef] [PubMed]

16. Ionascut-Nedelcescu, A.; Carlone, C.; Houdayer, A.; von Bardeleben, H.J.; Cantin, J.-L.; Raymond, S. Radiation Hardness of Gallium Nitride. *IEEE Trans. Nucl. Sci.* **2002**, *49*, 2733–2738. [CrossRef]
17. Polyakov, A.Y.; Pearton, S.J.; Frenzer, P.; Ren, F.; Liu, L.; Kim, J. Radiation effects in GaN materials and devices. *J. Mater. Chem. C* **2013**, *1*, 877–887. [CrossRef]
18. Belahsene, S.; Saqri, N.A.A.; Jameel, D.; Mesli, A.; Martinez, A.; Sanoit, J.; Ougazzaden, A.; Salvestrini, J.P.; Ramdane, A.; Henini, M. Analysis of Deep Level Defects in GaN p-i-n Diodes after Beta Particle Irradiation. *Electronics* **2015**, *4*, 1090–1100. [CrossRef]
19. Zheng, R.; Lu, J.; Liu, Y.; Li, X.; Xu, X.; He, R.; Tao, Z.; Gao, Y. Comparative study of GaN betavoltaic bettery based on p-n junction and Schottky barrier diode. *Radiat. Phys. Chem.* **2020**, *168*, 108595. [CrossRef]
20. Bouzid, F.; Pezzimenti, F.; Dehimi, L. Modelling and performance analysis of a GaN-based n/p junction betavoltaic cell. *Nucl. Instum. Methods Phys. Res. A* **2020**, *969*, 164103. [CrossRef]
21. Boguslawski, P.; Briggs, E.L.; Bernholc, J. Native defects in gallium nitride. *Phys. Rev. B* **1995**, *51*, 17255–17259. [CrossRef] [PubMed]
22. Alugubelli, S.R.; Fu, H.; Fu, K.; Liu, H.; Zhao, Y.; Ponce, F.A. Dopant profiling in p-i-n GaN structures using secondary electrons. *J. Appl. Phys.* **2019**, *126*, 015704. [CrossRef]
23. Cheng, Z.J.; San, H.S.; Feng, B.; Liu, B.; Chen, X.Y. High open-circuit voltage betavoltaic cell based on GaN pin homojunction. *Electron. Lett.* **2011**, *47*, 720–722. [CrossRef]
24. Aydin, S.; Kam, E. Investigation of nickel-63 radioisotope-powered GaN betavoltaic nuclear battery. *Int. J. Energy Res.* **2019**, *43*, 8725–8738. [CrossRef]
25. Zuo, G.; Zhou, J.; Ke, G. A Simple theoretical model for 63Ni betavoltaic battery. *Appl. Radiat. Isot.* **2013**, *82*, 119–125. [CrossRef]
26. Belghachi, A.; Bozkurt, K.; Moughli, H.; Ozdemir, O.; Amiri, B.; Talhi, A. A Model for Ni-63 Source for Betavoltaic Application. *Acta Phys. Pol. A* **2020**, *137*, 324–331. [CrossRef]
27. Wang, D.-F.; Shiwei, F.; Lu, C.; Motayed, A.; Jah, M.; Mohammad, S.N.; Jones, K.A.; Salamanca-Riba, L. Low-resistance Ti/Al/Ti/Au multilayer ohmic contact to n-GaN. *J. Appl. Phys.* **2001**, *89*, 6214–6217. [CrossRef]
28. Ho, J.-K.; Jong, C.-S.; Chiu, C.C.; Huang, C.-N.; Chen, C.-Y.; Shih, K.-K. Low-resistance ohmic contacts to p-type GaN. *Appl. Phys. Lett.* **1999**, *74*, 1275–1277. [CrossRef]
29. *Atlas User's Manual*; Silvaco International Inc.: Santa Clara, CA, USA, 2016.
30. Robertson, C.A.; Qwah, K.S.; Wu, Y.-R.; Speak, J.S. Modeling dislocation-related leakage currents in GaN p-n diodes. *J. Appl. Phys.* **2019**, *126*, 245705. [CrossRef]
31. Cho, H.K.; Kim, C.S.; Hong, C.-H. Electron capture behaviors of deep level traps in unintentionally doped and intentionally doped *n*-type GaN. *J. Appl. Phys.* **2003**, *94*, 1485–1489. [CrossRef]
32. Polyakov, A.Y.; Lee, I.-H.; Smirnov, N.B.; Govorkov, A.V.; Kozhukhova, E.A.; Pearton, S.J. Comparison of hole traps in n-GaN grown by hydride vapor phase epitaxy, metal organic chemical vapor deposition, and epitaxial lateral overgrowth. *J. Appl. Phys.* **2011**, *109*, 123701. [CrossRef]